Electronic Supplementary Material (ESI) for Dalton Transactions.
This journal is © The Royal Society of Chemistry 2022

Electronic Supporting Information

Gold(I) Complexes of Tetra-tert-butylcyclotetraphosphane

Content

1. Reaction of $[(AuCl)_2\{cyclo\text{-}(P^tBu)_4\}]$ (2) with PPh_3

4.45 mg (0.0054 mmol) $[(AuCl)_2\{cyclo\text{-}(P^tBu)_4\}]$ (**2**) and 1.04 mg (0.0040 mmol, 0.73 equiv.) PPh_3 were dissolved in 1 ml THF and stirred for 5 min. The reaction mixture was examined by $^{31}P\{^1H\}$ NMR spectroscopy (Fig. S1).

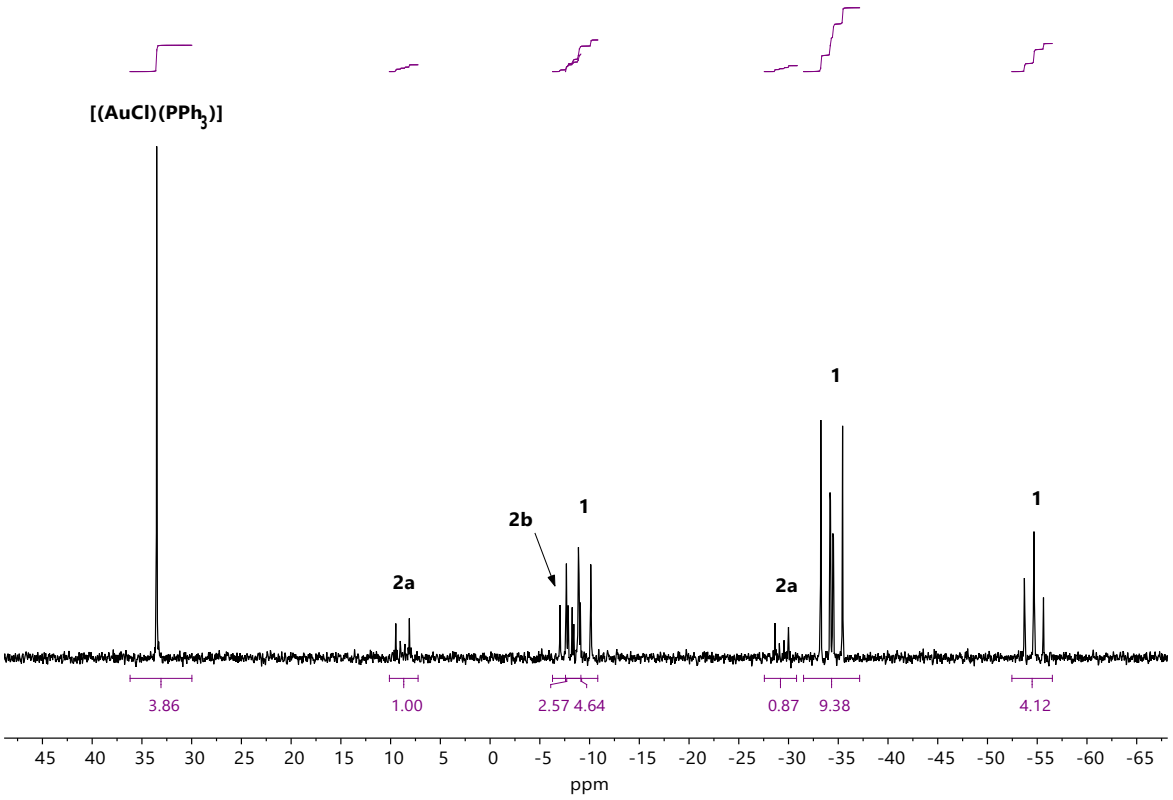

Fig. S1 $^{31}P\{^1H\}$ NMR spectrum (162 MHz) of the reaction mixture of **2** + PPh_3 in THF with lock to benzene-d^6 (capillary) ($[(AuCl)\{cyclo\text{-}(P^tBu)_4\}]$ (**1**), $[1,2\text{-}(AuCl)_2\{cyclo\text{-}(P^tBu)_4\}]$ (**2a**), $[1,3\text{-}(AuCl)_2\{cyclo\text{-}(P^tBu)_4\}]$ (**2b**)).

2. Identification of Oxidation Products

In the $^{31}P\{^1H\}$ NMR spectrum of $[(AuCl)_2\{cyclo\text{-}(P^tBu)_4\}]$ (**2**), three additional AM_2X spin systems are observed. One of them can be assigned to the complex $[(AuCl)\{cyclo\text{-}(P^tBu)_4\}]$ (**1**), the other two to $[(AuCl)_3\{cyclo\text{-}(P^tBu)_4\}]$ (**3**) and supposedly a gold(I) complex with an oxidised ligand. To identify the corresponding compound, several oxidation studies on the NMR scale were conducted. First, *cyclo*-$(P^tBu)_4$ was oxidised in benzene-d^6 to give the oxidised species *cyclo*-$(P^tBu)_4O_{1–3}$ (see Section 2.1) which were already reported.[1] Subsequent addition of one equivalent of [AuCl(tht)] gives the corresponding mononuclear gold(I) complexes of *cyclo*-$(P^tBu)_4O_{1–3}$ (see Section 2.2). The addition of another equivalent [AuCl(tht)] should yield the dinuclear gold(I) complexes of *cyclo*-$(P^tBu)_4O_{1–2}$ (see Section 2.3). Indeed, one of the AM_2X spin systems observed in the $^{31}P\{^1H\}$ NMR spectrum of **2** as mentioned above could be assigned to a dinuclear gold(I) complex of the monoxide *cyclo*-$(P^tBu)_4O$, enabling the correct assignment of the $^{31}P\{^1H\}$ NMR spectrum of **3**.

2.1. Preparation of the Oxides *cyclo*-(P^{t}Bu)$_4$O$_{1–3}$

24.16 mg (0.069 mmol) *cyclo*-(P^{t}Bu)$_4$ (**L**) were dissolved in 0.5 ml benzene-*d*^{6} and oxidised with 0.01 ml of a ^{t}BuOOH solution (>5.5 M in decane). The solution was stirred for 1 h at ambient temperature. The reaction mixture (Scheme S1) was examined by ^{31}P{^{1}H} NMR spectroscopy (Fig. S2).

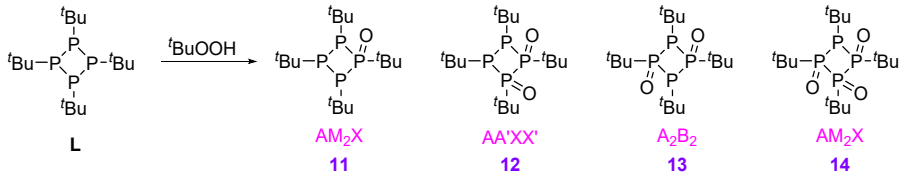

Scheme S1 Reaction of **L** with ^{t}BuOOH gives the oxides *cyclo*-(P^{t}Bu)$_4$O$_{1–3}$ (**11**–**14**).[1] The spin systems are denoted in pink.

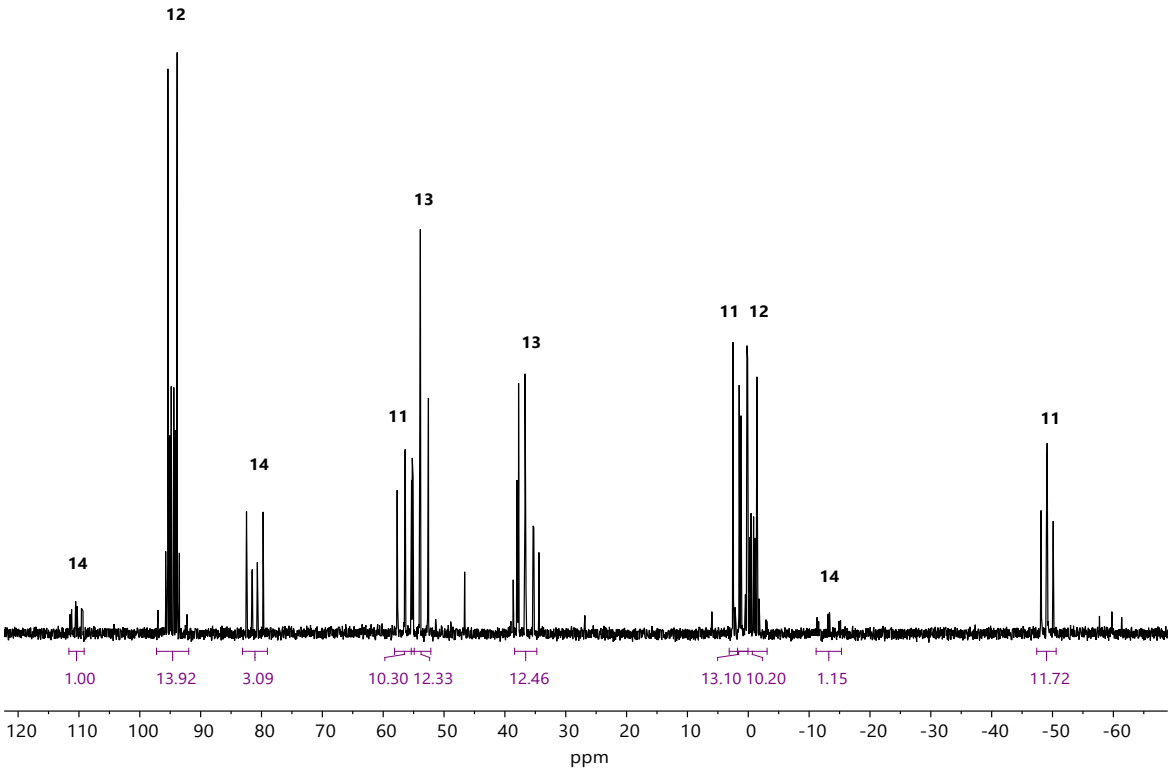

Fig. S2 ^{31}P{^{1}H} NMR spectrum (162 MHz) of the mixture of the oxides *cyclo*-(P^{t}Bu)$_4$O$_{1–3}$ in benzene-*d*^{6}. The assignment of the resonances follows the literature (Scheme S1).[1]

2.2. Preparation of [(AuCl){*cyclo*-(P^{t}Bu)$_4$}O$_{1–3}$]

22.0 mg (0.069 mmol, 1 equiv. based on **L**) [AuCl(tht)] were added to the solution of oxides *cyclo*-(P^{t}Bu)$_4$O$_{1–3}$ described above (Section 2.1). The reaction mixture (Scheme S2) was examined by ^{31}P{^{1}H} NMR spectroscopy (Fig. S3). Only compounds **21** and **31** could be observed and identified based on their spin systems, their chemical shifts and their abundancy related to those of the oxides **11**–**14** in Section 2.1.

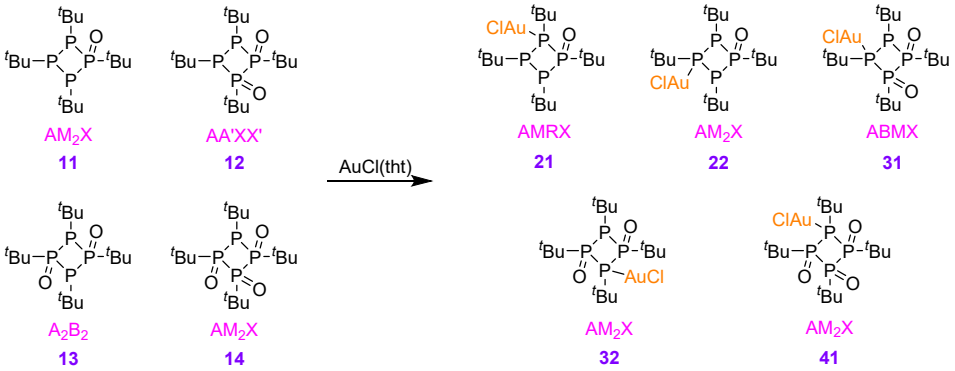

Scheme S2 The reaction of the oxides with [AuCl(tht)] may form the complexes **21**, **22**, **31**, **32** and **41**. However, only **21** and **31** were observed by $^{31}P\{^{1}H\}$ NMR spectroscopy (Fig. S3). The spin systems are denoted in pink.

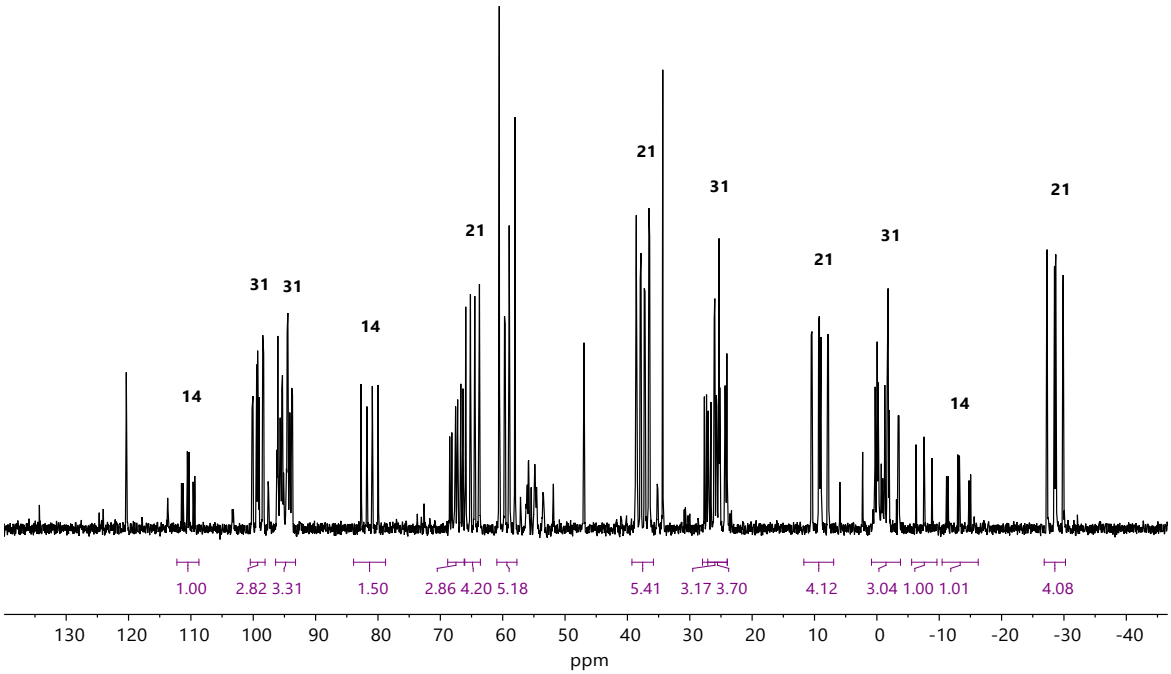

Fig. S3 $^{31}P\{^{1}H\}$ NMR spectrum (162 MHz) after the addition of 1 equiv. [AuCl(tht)] to the solution of the oxides *cyclo*-$(P^tBu)_4O_{1–3}$ in benzene-d^6.

2.3. Preparation of $[(AuCl)_2\{cyclo\text{-}(P^tBu)_4\}O_{1–2}]$

Further 20.41 mg (0.064 mmol, 0.93 equiv. based on **L**) [AuCl(tht)] were added to the solution of Section 2.2. The reaction mixture (Scheme S3) was examined by $^{31}P\{^{1}H\}$ NMR spectroscopy (Fig. S4). Among the hypothetic products, only **24** could be observed.

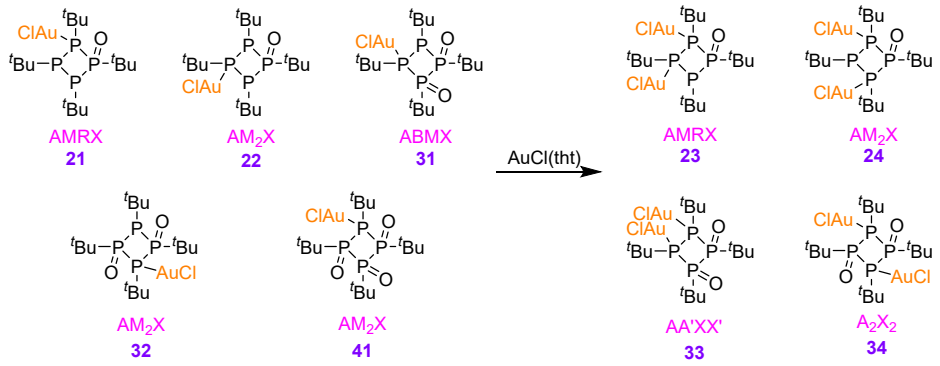

Scheme S3 Addition of one further equivalent [AuCl(tht)] may form the compounds **23**, **24**, **33** and **34**. The spin systems are denoted in pink. Only **24** could be identified among the possible products under the given reaction conditions.

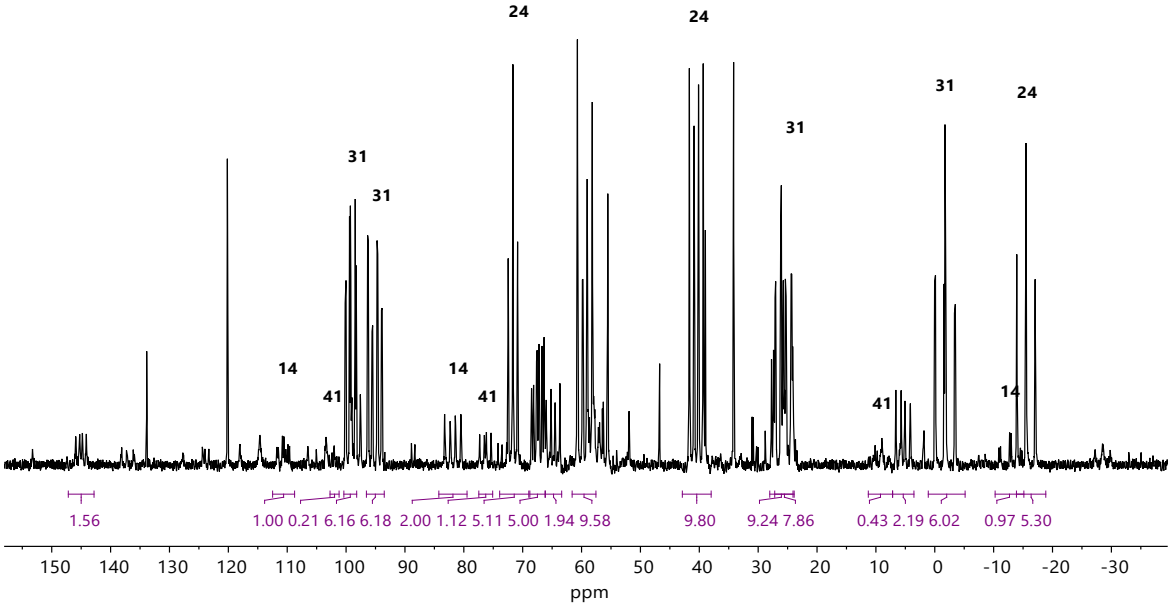

Fig. S4 $^{31}P\{^{1}H\}$ NMR spectrum (162 MHz) after the addition of one further equivalent [AuCl(tht)] to the solution of Section 2.2 in benzene-d^6.

The $^{31}P\{^{1}H\}$ NMR parameters of **24** and **31** were determined by automated line-shape analysis (Fig. S5). No *R*-values are given due to strong overlap. However, as the spin systems are almost first order, the parameters can be considered as reliable, although the $^{2}J_{PP}$ coupling J_{AX} is not resolved anymore due to strong line broadening.

24: $^{31}P\{^{1}H\}$ NMR (162 MHz, benzene-d^6): AM_2X spin system (C_1): δ_A = 71.62, δ_M = 40.46, δ_X = –15.51 ppm; J_{AM} = –129.11 Hz, J_{AX} = 0.01 Hz, J_{MX} = –253.16 Hz; H = 14.03 Hz.

31: $^{31}P\{^{1}H\}$ NMR (162 MHz, benzene-d^6): ABMX spin system (C_1): δ_A = 99.15, δ_B = 95.10, δ_M = 25.65, δ_X = –1.74 ppm; J_{AB} = –120.44 Hz, J_{AM} = –159.22 Hz, J_{AX} = 26.71 Hz, J_{BM} = 20.19 Hz, J_{BX} = –263.27 Hz, J_{MX} = –285.61 Hz; H_A = H_B = H_X = 10 Hz, H_M = 11 Hz.

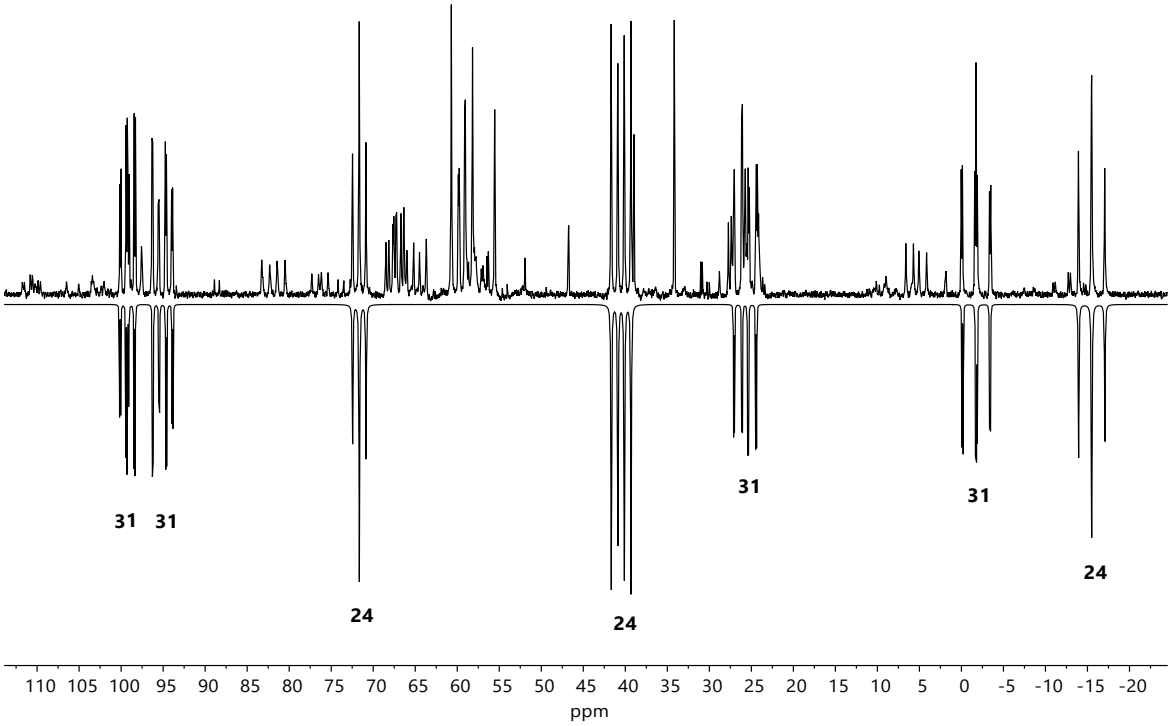

Fig. S5 Calculated $^{31}P\{^{1}H\}$ NMR spectra (162 MHz) (bottom) of **24** and **31**.

3. Infrared Spectra of 4

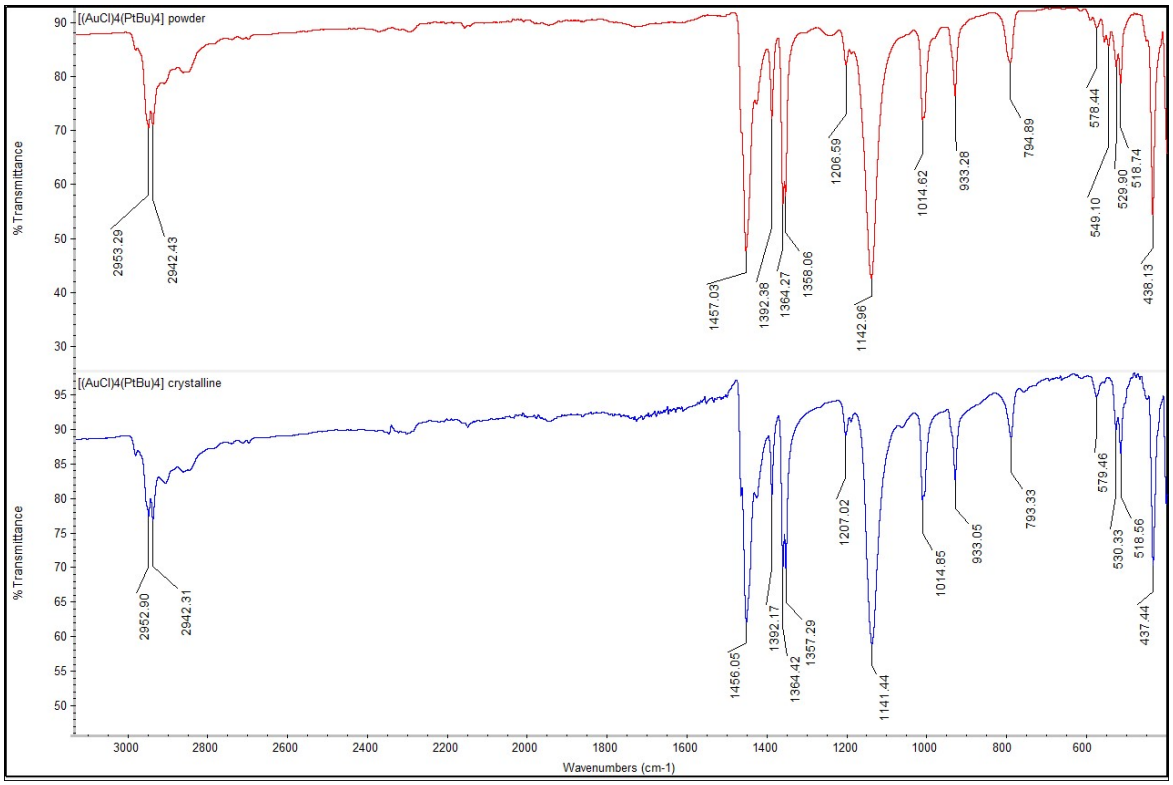

Fig. S6 Comparison of the IR spectra of **4**. Top: precipitate of **4**, bottom: single crystals of **4**. Apart from the vibration at 549 cm^{-1}, the spectra look alike.

4. X-Ray Crystallography

4.1. Single Crystal X-Ray Diffraction

Crystallographic data obtained from single-crystal X-ray diffraction are summarised in Table S1.

4.1.1. Detailed Description of the Relative Abundancies in the Single Crystal Structure of 2.

The disorder in the crystal structure of **2b** (Fig. S7) which describes the coordination of the third Au–Cl fragment (Au3–Cl3 and Au3'–Cl3') was refined to 3.43 %. To calculate the relative abundancies of the oligonuclear complexes the binomial coefficient was used regarding an excerpt with the two symmetry-independent molecules where p is the refined percentage of the disorder and P is the relative abundancy. The calculation is based on the smallest repeating unit, but because of the law of large numbers, the obtained abundancies are valid for the whole crystal.

Case 1:

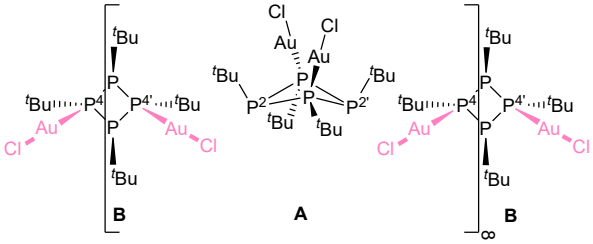

Compound **2** **2** **2**

Case 2:

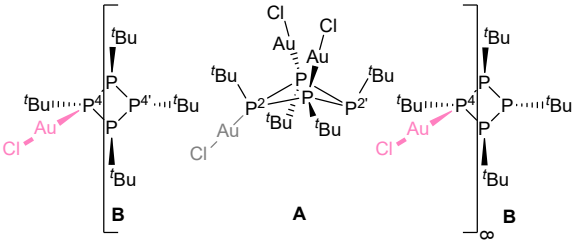

Compound **1** **3** **1**

Case 3:

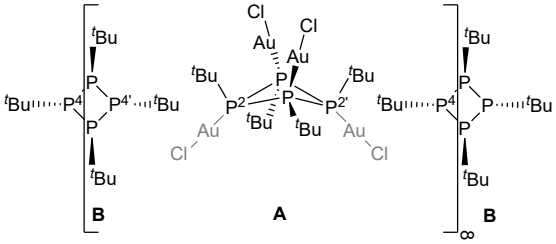

Compound **L** **4** **L**

P(**2**) = P(**case 1**) = $\binom{2}{2} p^0 (1-p)^{2-0} = (1-p)^2 = (0.9657)^2 = 93.26\,\%$

P(**1**) = P(**3**) = ½ P(**case 2**) = ½ $\binom{2}{1} p^1 (1-p)^{2-1} = ½ \cdot 2 \cdot p \cdot (1-p) = 0.0343 \cdot (0.9657) = 3.31\,\%$

P(**L**) = P(**4**) = ½ P(**case 3**) = ½ $\binom{2}{0} p^2 (1-p)^{2-2} = ½ \cdot p^2 = ½ \cdot (0.0343)^2 = 0.06\,\%$

P(**L**) + P(**1**) + P(**2**) + P(**3**) + P(**4**) = 100%

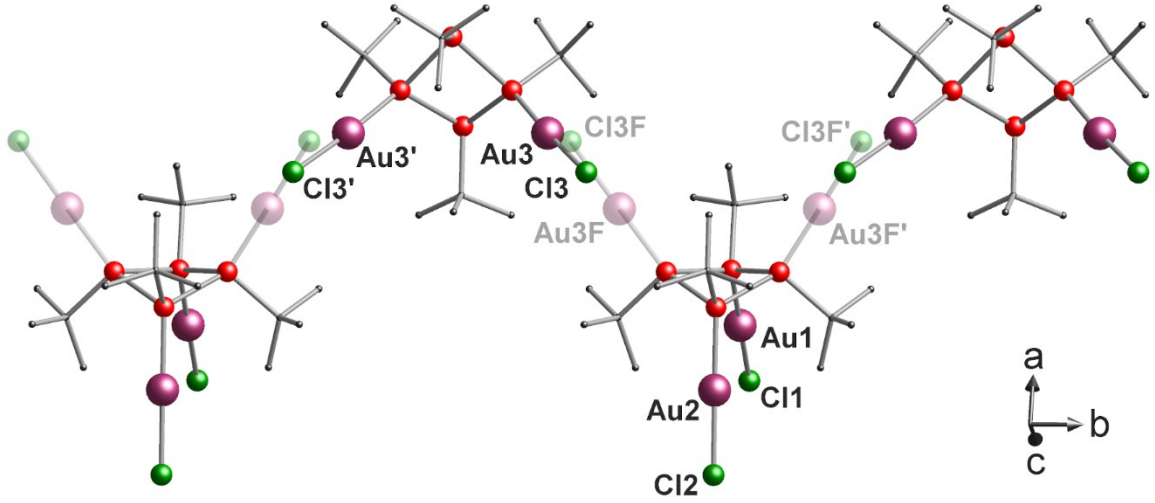

Fig. S7 Segment of the crystal structure of complex **2b** which shows the discussed disorder with the disordered fragments drawn transparently.

Table S2 Summary of Crystallographic Data Obtained from Single-Crystal X-Ray Diffraction.

Compound	*cyclo*-$(P^tBu)_4 \cdot 0.5\,THF$	**1**–α†	**1**–β	**2b**	**3** $\cdot 2.5\,C_7H_8$	**4**
Empirical formula	$C_{18}H_{40}O_{0.5}P_4$	$C_{16}H_{36}AuClP_4$	$C_{16}H_{36}AuClP_4$	$C_{16}H_{36}Au_2Cl_2P_4$	$C_{33.5}H_{56}Au_3Cl_3P_4$	$C_{16}H_{36}Au_4Cl_4P_4$
Formula weight	388.38	584.74	584.74	817.16	1279.91	1281.99
Temperature [K]	130(2)	140(2)	293(2)‡	130(2)	220(2)‡	130(2)
Wavelength [pm]	71.073	71.073	71.073	71.073	71.073	71.073
Crystal system	Monoclinic	Monoclinic	Monoclinic	Orthorhombic	Monoclinic	Monoclinic
Space group	*C*2/*c*	$P2_1/c$	$P2_1/m$	*Pnma*	*C*2/*c*	*C*2/*c*
Unit cell						
a [Å]	23.5187(4)	10.8779(1)	9.043(1)	12.5495(1)	19.0733(4)	10.5127(2)
b [Å]	10.9722(2)	48.9793(6)	10.940(2)	14.9777(2)	24.8181(6)	15.8076(2)
c [Å]	18.0895(3)	13.1705(2)	12.499(1)	26.6883(3)	17.9778(3)	17.1149(2)
α [deg]	90	90	90	90	90	90
β [deg]	97.265(2)	89.996(1)	101.55(1)	90	98.934(2)	101.024(1)
γ [deg]	90	90	90	90	90	90
Volume [Å^3]	4630.55(14)	7017.1(2)	1211.4(3)	5016.4(1)	8406.8(3)	2791.68(7)
Z	4	12	2	8	8	4
ρ (calc) [Mg/m^3]	1.114	1.660	1.603	2.164	2.023	3.050
μ mm^{-1}	0.326	6.674	6.443	12.153	10.810	21.572
F(000)	1696	3456	576	3072	4840	2304
Crystal size [mm^3]	0.20 x 0.20 x 0.10	0.33 x 0.30 x 0.19	0.36 x 0.25 x 0.16	0.23 x 0.21 x 0.11	0.22 x 0.03 x 0.03	0.19 x 0.12 x 0.07
Θ min / *Θ* max [deg]	2.270 / 32.303	1.987 / 26.646	2.496 / 29.311	2.228 / 30.227	2.294 / 28.518	2.357 / 34.810
Index ranges	$-35 \le h \le 33$	$-13 \le h \le 12$	$-12 \le h \le 11$	$-17 \le h \le 17$	$-24 \le h \le 25$	$-16 \le h \le 16$
	$-16 \le k \le 16$	$-61 \le k \le 61$	$-14 \le k \le 14$	$-21 \le k \le 21$	$-32 \le k \le 31$	$-24 \le k \le 24$
	$-27 \le l \le 27$	$-16 \le l \le 16$	$-14 \le l \le 16$	$-36 \le l \le 36$	$-23 \le l \le 23$	$-27 \le l \le 25$
Reflections collected	46765	59314	12440	67611	36462	21549
Independent reflections [R(int)]	7863 [0.0374]	13844 [0.0411]	3061 [0.0649]	7421 [0. 0517]	9694 [0.0734]	5710 [0.0215]
Completeness [%] (*Θ*) [deg]	100 (25.242)	99.9 (25.350)	99.9 (25.350)	100 (28.285)	99.9 (26.360)	100 (33.140)
T_{Max} / T_{Min}	1.00000 / 0.97254	0.432 / 0.237	0.498 / 0.182	0.349 / 0.098	0.751 / 0.394	0.290 / 0.139
Restraints / parameters	4 / 238	0 / 632	1 / 117	2 / 265	408 / 512	0 / 133
Goodness-of-fit on F^2	1.046	1.126	1.069	1.086	1.008	1.163
R_1, wR_2 [I > 2σ(*I*)]	0.0364, 0.0862	0.0300, 0.0602	0.0393, 0.0843	0.0290, 0.0553	0.0475, 0.0686	0.0197, 0.0357
R indices (all data)	0.0473, 0.0916	0.0319, 0.0610	0.0630, 0.0977	0.0379, 0.0581	0.1009, 0.0822	0.0228, 0.0363
Residual electron density [e $\cdot$ Å^{-3}]	0.429 / –0.393	0.986 / –0.742	0.624 / –0.793	2.470 / –1.033	1.121 / –0.920	0.906 / –1.598
CCDC number	2131408	2143199	2143200	2143201	2143202	2143203

† Two component pseudomerohedral twin. Twin law by rows –1.00 0.00 0.00 0.00 –1.00 0.00 0.00 0.00 1.00; Twin domain ratio: 0.6087(5) : 0.3913(5).

‡ As a result of a phase transition the data was recorded at elevated temperatures to avoid twinning.

4.2. Powder X-Ray Diffraction

Powder X-ray diffraction data (Table S3) were collected on a STADI P diffractometer (STOE) with a silicon solid-state detector Mythen-1K (DECTRIS) at room temperature. The radiation source was a copper anode (Cu-K_α, λ = 1.540598 Å) combined with a germanium single crystal monochromator. Samples were measured in sealed glass capillaries (inner diameter 0.3 mm or 0.5 mm, HILGENBERG) with Debye-Scherrer geometry. The theoretical powder pattern from the single crystal structures was calculated using MERCURY.[2] The Rietveld analysis for complexes **1** and **4** was performed with a fundamental parameter approach using the software TOPAS[3] version 5 (Bruker). The background was modelled by a polynomial function (6th order) of the Chebyshev type. Peak shapes were described by the fundamental parameter approach. Separate isotropic thermal parameters were assigned and allowed to freely refine for gold and all remaining elements. The molecule was treated as a rigid body for which the molecular parameters were taken from the single crystal structures of **1** and **4**, only allowing the torsion angles of the P–P bonds to be refined. A summary of the powder X-ray is given in Table S3.

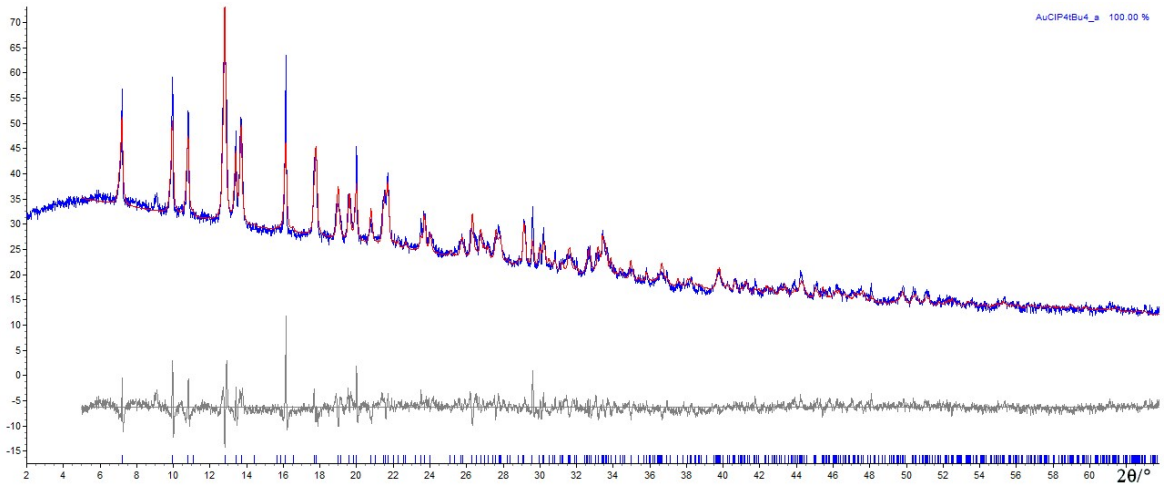

Fig. S8 Rietveld refinement plots for polymorph **1**–β with peak markers and difference plot at the bottom. The peak at 2θ = 9° corresponds to an unknown impurity and not to the structures of the ligand *cyclo*-(P^{t}Bu)$_4$ (**L**) or the dinuclear complex **2**.

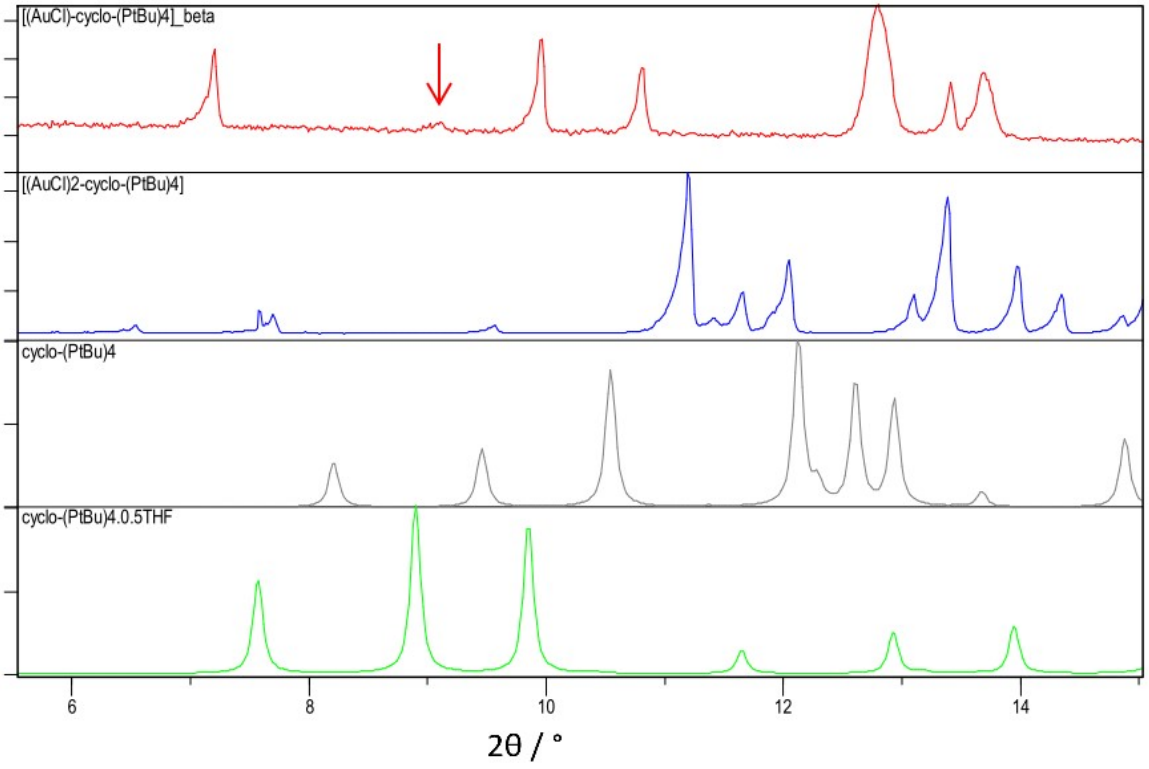

Fig. S9 Comparison of PXR diffractograms. From top to bottom: complex **1**–β, complex **2**, *cyclo*-(P^tBu)$_4$ (**L**) (simulated pattern from single crystal structure) and *cyclo*-(P^tBu)$_4$·0.5 THF (simulated pattern from single crystal structure). As can be seen, the peak at 2θ = 9° in the PXR diffractogram of **1**–β cannot be assigned to the structure of **2** or *cyclo*-(P^tBu)$_4$.

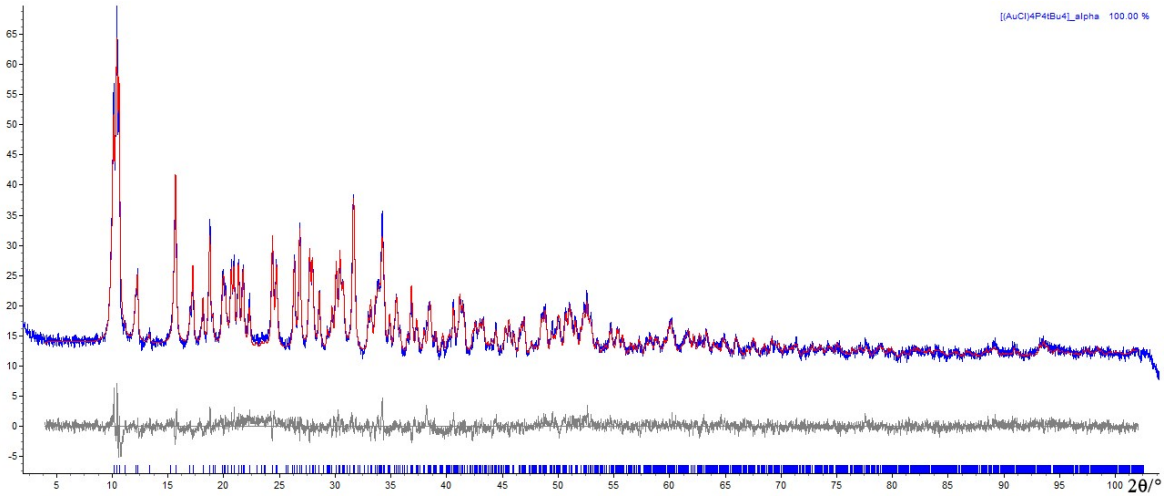

Fig. S10 Rietveld refinement plots for polymorph **4**–α (crystals grown by layering) with peak markers and difference plot at the bottom.

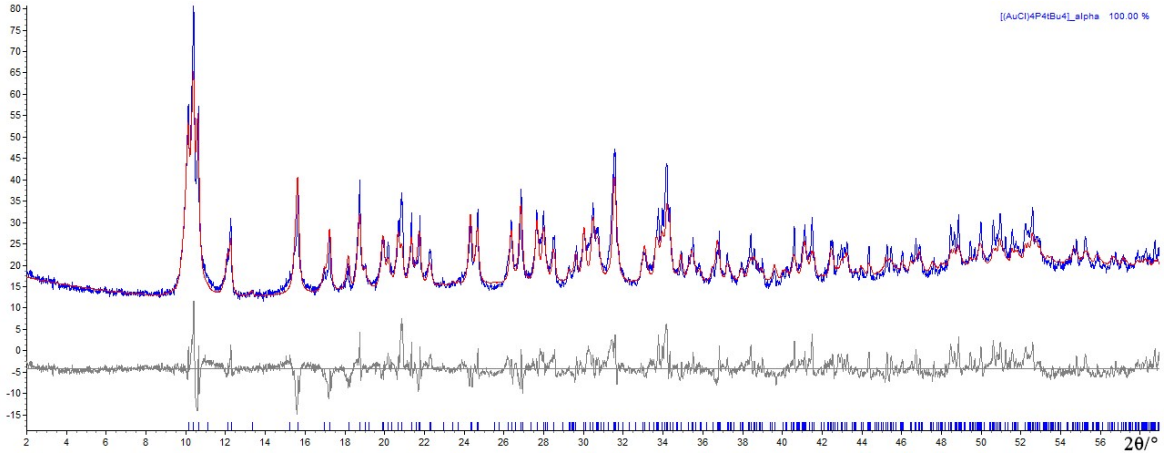

Fig. S11 Rietveld refinement plots for complex **4**–α (powder sample obtained by alternative procedure) with peak markers and difference plot at the bottom.

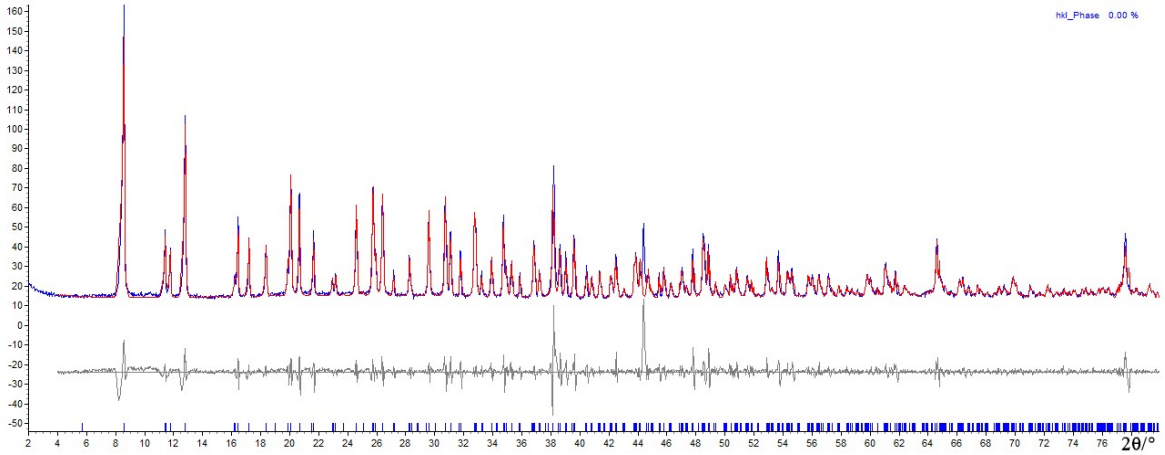

Fig. S12 LeBail refinement plots for the second polymorph or solvatomorph of complex **4** (**4**–β) with peak markers and difference plot at the bottom.

Table S3 Summary of Crystallographic Data obtained from Powder X-Ray Diffraction.

Compound	**1**–α (powder)	**4** (powder)	**4** (crystals)	**4** (second polymorph/solvatomorph)
Empirical formula	$C_{16}H_{36}Au_1Cl_1P_4$	$C_{16}H_{36}Au_4Cl_4P_4$	$C_{16}H_{36}Au_4Cl_4P_4$	–
Formula weight	584.74	1281.99	1281.99	–
Temperature [K]	298	298	298	298
Wavelength [pm]	154.0598	154.0598	154.0598	154.0598
Crystal system	Monoclinic	Monoclinic	Monoclinic	Tetragonal
Space group	$P2_1/m$	$C2/c$	$C2/c$	$P4/nnc$
Unit cell				
a [Å]	9.0619	10.6347	10.6250	10.9278
b [Å]	10.9843	15.9089	15.9049	
c [Å]	12.5184	17.2976	17.3169	30.9825
α [deg]	90	90	90	90
β [deg]	101.425	101.104	100.822	90
γ [deg]	90	90	90	90
Volume [Å^3]	1221.371	2871.736	2874.336	3699.825
Z	2	4	4	–
Θ min / Θ max [deg]	5 / 63	2 / 100	2 / 60	2 / 80
Beq(Au) [Å^2]	1.779	1.784	1.001	–
Beq(all) [Å^2]	9.927	1.002	1.003	–
Goodness-of-fit	2.259341	1.522759	3.783901	5.180476
R_{Bragg} [%]	4.017274	17.20614	11.76124	3.291281
R_{exp} [%]	4.155916	6.308893	4.782182	4.536968
R_{wp} [%]	9.389630	9.606922	18.09530	23.50365
R_p [%]	6.895997	7.480211	13.77888	15.28656

5. Quantum Chemical Calculations

All calculations were carried out with DFT using the program ORCA[4] (version 5.0.1). For all calculations, the convergence criterion was set to tight SCF convergence and the atom-pairwise dispersion correction based on tight binding partial charges (D4)[5,6] was used. Relativistic effects were considered using Zero Order Regular Approximation (ZORA).[7] Furthermore, the RIJDX approximation was used to speed up the calculations. In all cases the free Gibbs energy ΔG was calculated using a numerical frequency analysis. In each case only positive Eigenvalues in the Hesse matrix confirmed an energetic minimum.

In analogy to our previous study,[8] different combinations of functionals and basis sets were tested. For all calculations, the TPSSh functional[9,10] in combination with the def2-TZVP[11] basis set was used because this showed the best agreement with the molecular parameters obtained from the single crystal X-ray diffraction measurements. The simulation of the solvent environment was performed using the conductor-like polarisable continuum model (C-PCM)[12] model. For calculations of all molecules the solvent was set to tetrahydrofuran (THF). Additional calculations were run for the dinuclear complexes for which the solvents were set to benzene, toluene, and acetonitrile.

The calculated Gibbs energies and Gibbs reaction energies are listed in Table S4 and Table S5.

Table S4 Calculated Gibbs energies (given in Hartree) for the molecules in this article.

Compound	*G*
cyclo-($P^tBu)_4$ (**L**)	–1996.9
[(AuCl){*cyclo*-($P^tBu)_4$}] (**1**)	–2593.2
[1,2-$(AuCl)_2${*cyclo*-($P^tBu)_4$}] (**2a**)	–3189.4
[1,3-$(AuCl)_2${*cyclo*-($P^tBu)_4$}] (**2b**)	–3189.4
[$(AuCl)_3${*cyclo*-($P^tBu)_4$}] (**3**)	–3785.6
[$(AuCl)_4${*cyclo*-($P^tBu)_4$}] (**4**)	–4381.8
[AuCl(tht)]	–1151.7
tht	–555.5

Table S5 Gibbs reaction energies (given in kJ mol^{-1}) for the reactions in this article

Reaction			Δ*G*
cyclo-($P^tBu)_4$ + [AuCl(tht)]	→	[(AuCl){*cyclo*-($P^tBu)_4$}] + tht	–63.2
[(AuCl){*cyclo*-($P^tBu)_4$}] + [AuCl(tht)]	→	[1,2-$(AuCl)_2${*cyclo*-($P^tBu)_4$}] + tht	–46.7
[1,2-$(AuCl)_2${*cyclo*-($P^tBu)_4$}] + [AuCl(tht)]	→	[$(AuCl)_3${*cyclo*-($P^tBu)_4$}] + tht	–36.4
[$(AuCl)_3${*cyclo*-($P^tBu)_4$}] + [AuCl(tht)]	→	[$(AuCl)_4${*cyclo*-($P^tBu)_4$}] + tht	–27.7
2 [(AuCl){*cyclo*-($P^tBu)_4$}]	→	[1,2-$(AuCl)_2${*cyclo*-($P^tBu)_4$}] + *cyclo*-($P^tBu)_4$	0.006
2 [1,2-$(AuCl)_2${*cyclo*-($P^tBu)_4$}]	→	[$(AuCl)_3${*cyclo*-($P^tBu)_4$}] + [(AuCl){*cyclo*-($P^tBu)_4$}]	0.004
2 [$(AuCl)_3${*cyclo*-($P^tBu)_4$}]	→	[$(AuCl)_4${*cyclo*-($P^tBu)_4$}] + [1,2-$(AuCl)_2${*cyclo*-($P^tBu)_4$}]	0.003
[1,2-$(AuCl)_2${*cyclo*-($P^tBu)_4$}]	→	[1,3-$(AuCl)_2${*cyclo*-($P^tBu)_4$}] (in benzene)	–0.5
[1,2-$(AuCl)_2${*cyclo*-($P^tBu)_4$}]	→	[1,3-$(AuCl)_2${*cyclo*-($P^tBu)_4$}] (in toluene)	–0.6
[1,2-$(AuCl)_2${*cyclo*-($P^tBu)_4$}]	→	[1,3-$(AuCl)_2${*cyclo*-($P^tBu)_4$}] (in THF)	–3.0
[1,2-$(AuCl)_2${*cyclo*-($P^tBu)_4$}]	→	[1,3-$(AuCl)_2${*cyclo*-($P^tBu)_4$}] (in MeCN)	–2.5
cyclo-($P^tBu)_4$ + 2 [AuCl(tht)]	→	[1,2-$(AuCl)_2${*cyclo*-($P^tBu)_4$}] + 2 tht	–109.9
cyclo-($P^tBu)_4$ + 3 [AuCl(tht)]	→	[$(AuCl)_3${*cyclo*-($P^tBu)_4$}] + 3 tht	–146.3
cyclo-($P^tBu)_4$ + 4 [AuCl(tht)]	→	[$(AuCl)_4${*cyclo*-($P^tBu)_4$}] + 4 tht	–174.1

6. Differential Thermal Analysis of [(AuCl){*cyclo*-($P^tBu)_4$}] (1)

TG-DTA was performed with a STA 449F1 instrument (Netzsch) under argon as protective gas and 20 K/min heating rate in an Al_2O_3 crucible. Above 196 °C, thermolysis of **1** leads to the formation of elemental gold with a residual mass of 33.67 % (calculated 33.68 %).

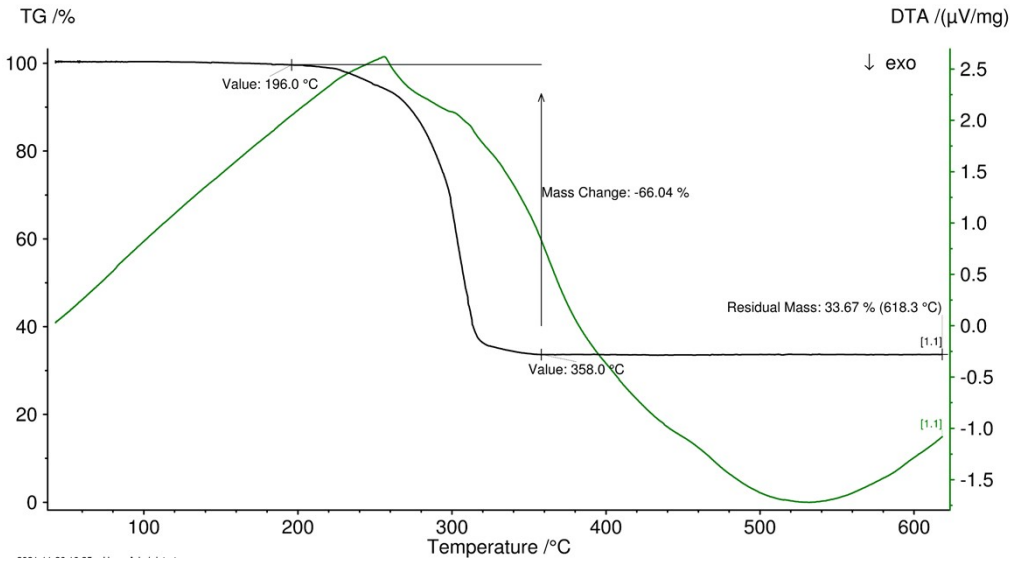

Fig. S13 TG-DTA analysis of **1**.

7. NMR Spectra

All NMR spectra have been recorded in benzene-d^6 at 25 °C unless stated otherwise. δ_{mean} at 25 °C can be correlated to the number of gold(I) chloride fragments in compounds *cyclo*-(P^tBu)$_4$ (**L**) and **1**–**3** (Table S6 and Diagram S1).

Table S6 Correlation between n and δ_{mean} in the $^{31}P\{^1H\}$ NMR spectra of [(AuCl)$_n${*cyclo*-(P^tBu)$_4$}] (n = 0–3) in benzene-d^6 at 25 °C and the chemical shift of **4**.

Compound	n	δ_{mean}
L	0	–57.70
1	1	–33.17
2	2	–10.08
3	3	11.48
4	4	29.3*

* This value was determined by $^{31}P\{^1H\}$ CP MAS NMR.

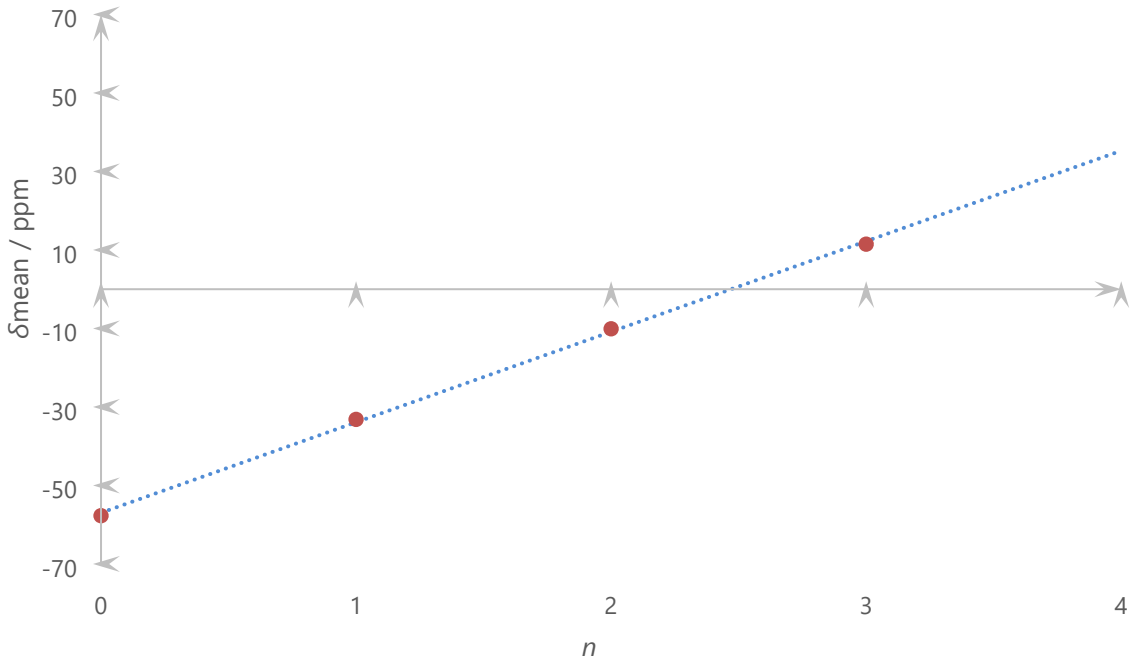

Diagram S1 Linear fit of δ_{mean} at 25 °C (red dots) against *n* in the compounds [(AuCl)$_n${*cyclo*-(P^{t}Bu)$_4$}] (*n* = 0–3) (**L**, **1**–**3**) and the experimental value of **4** (arithmetic mean), determined by ^{31}P{^{1}H} (CP-MAS) NMR (blue triangle, s. Fig. S26).

7.1. [(AuCl){*cyclo*-(P^{t}Bu)$_4$}] (1)

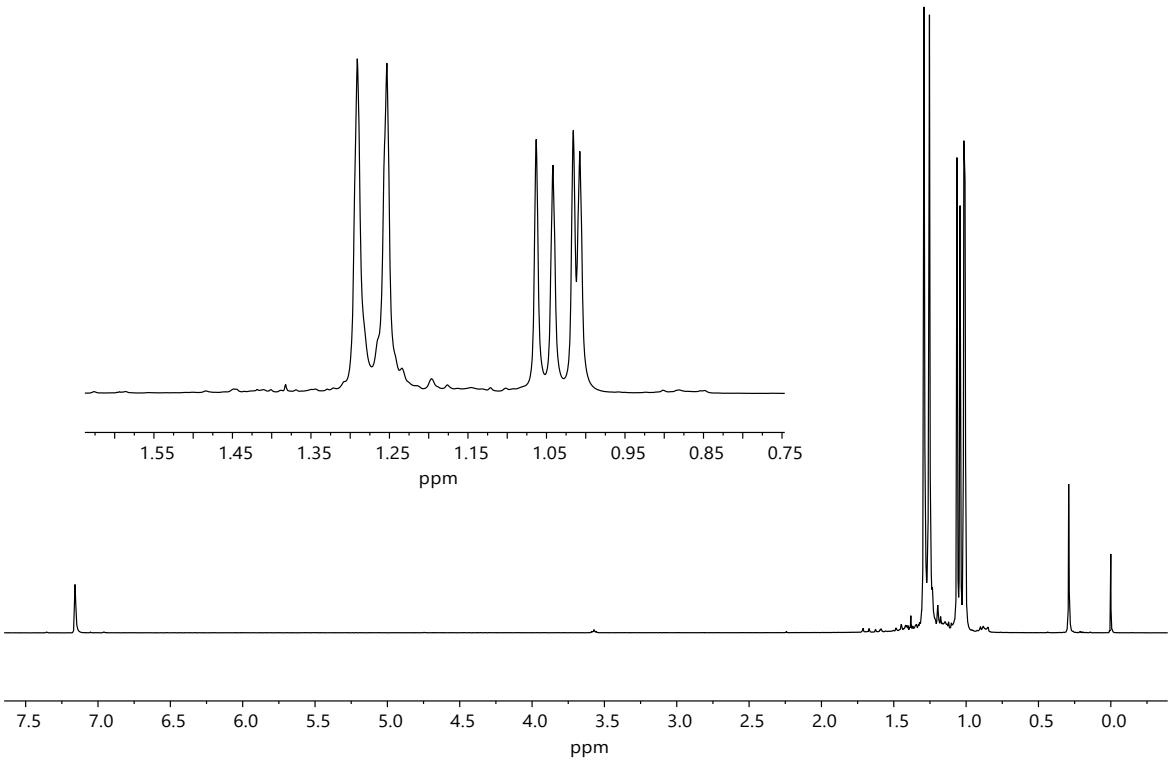

Fig. S14 ^{1}H NMR spectrum (400 MHz) of **1**.

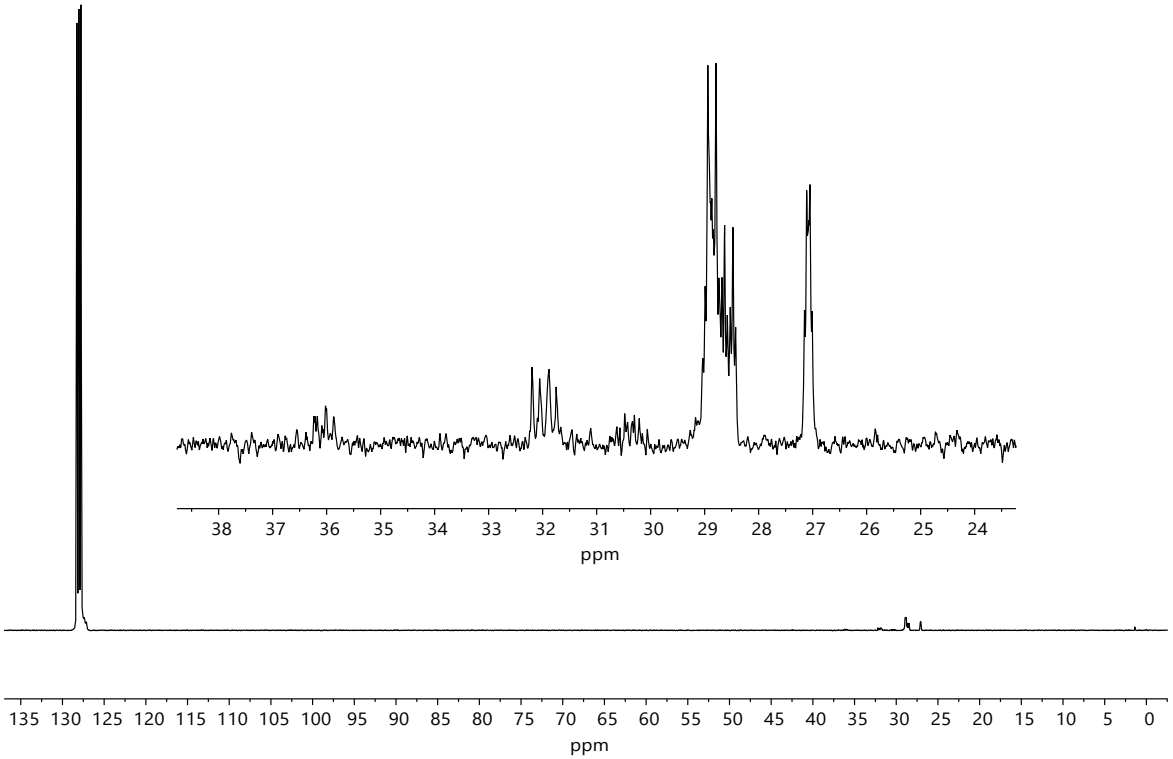

Fig. S15 $^{13}C\{^{1}H\}$ NMR spectrum (101 MHz) of **1**.

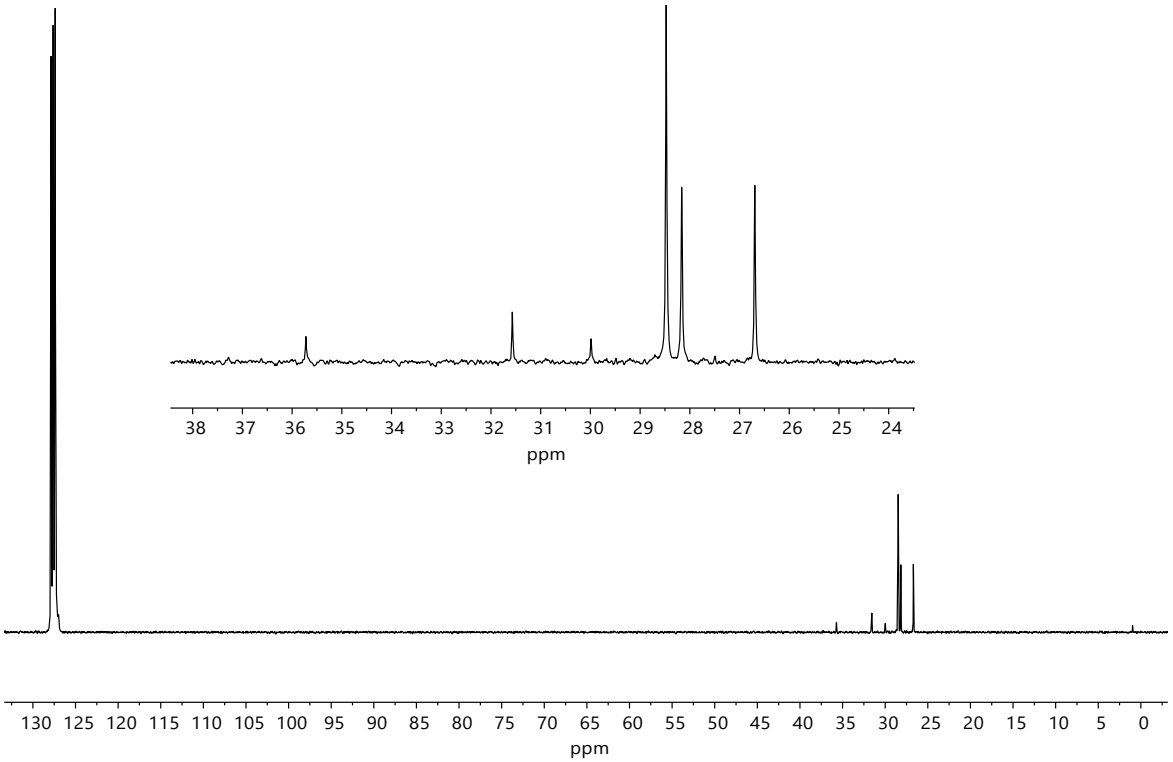

Fig. S16 $^{13}C\{^{1}H,^{31}P\}$ NMR spectrum (101 MHz) of **1** at 28 °C.

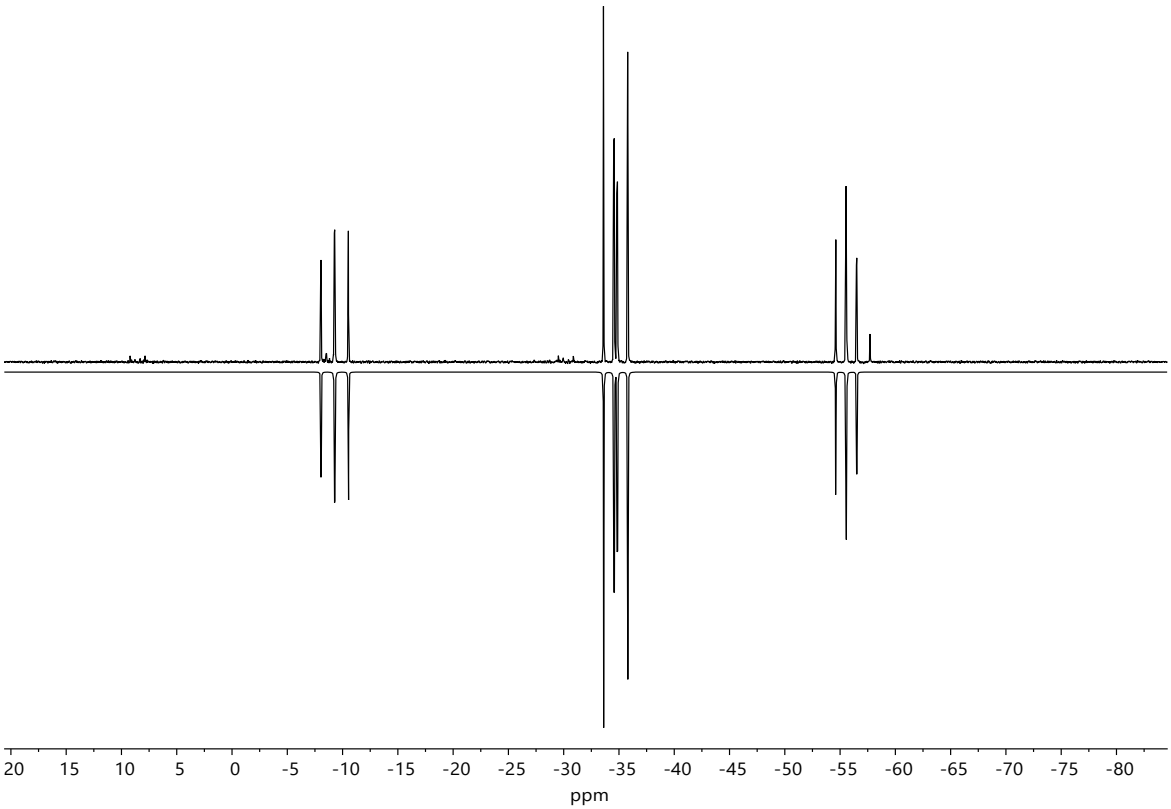

Fig. S17 Experimental (top) and simulated (bottom) $^{31}P\{^{1}H\}$ NMR spectra (162 MHz) of **1**.

7.2. $[(AuCl)_2\{cyclo\text{-}(P^tBu)_4\}]$ (2)

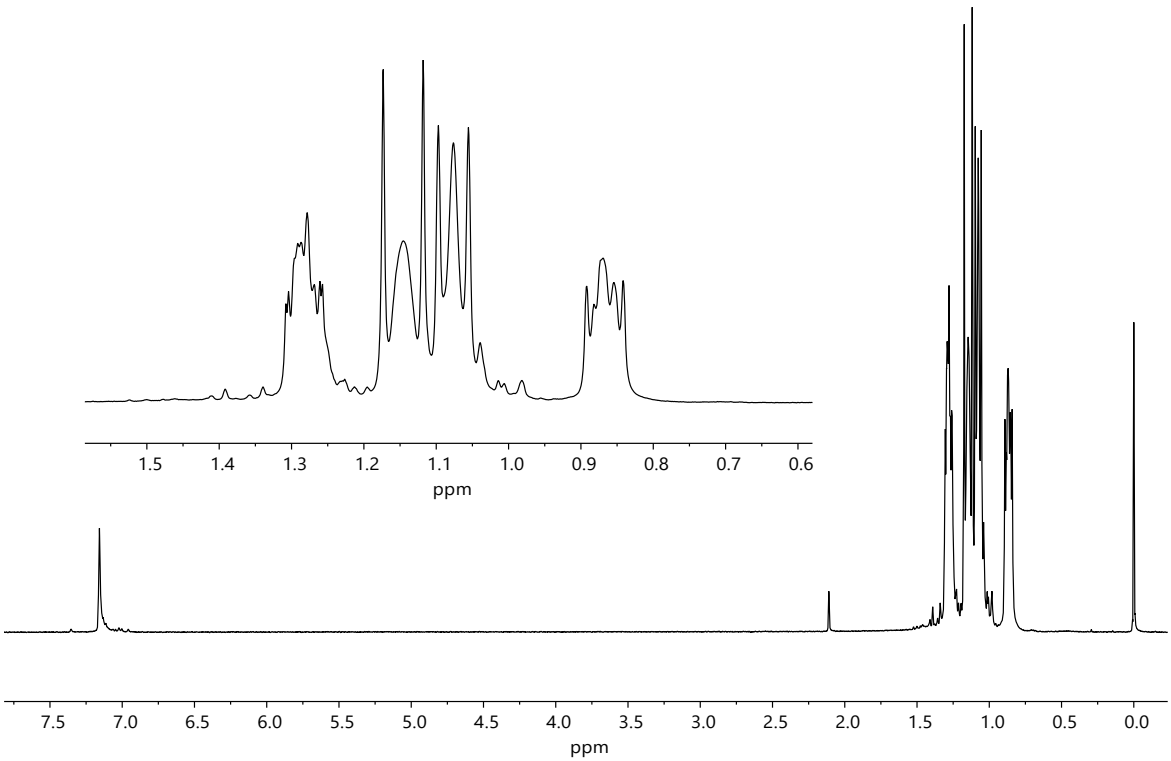

Fig. S18 ^{1}H NMR spectrum (400 MHz) of **2**.

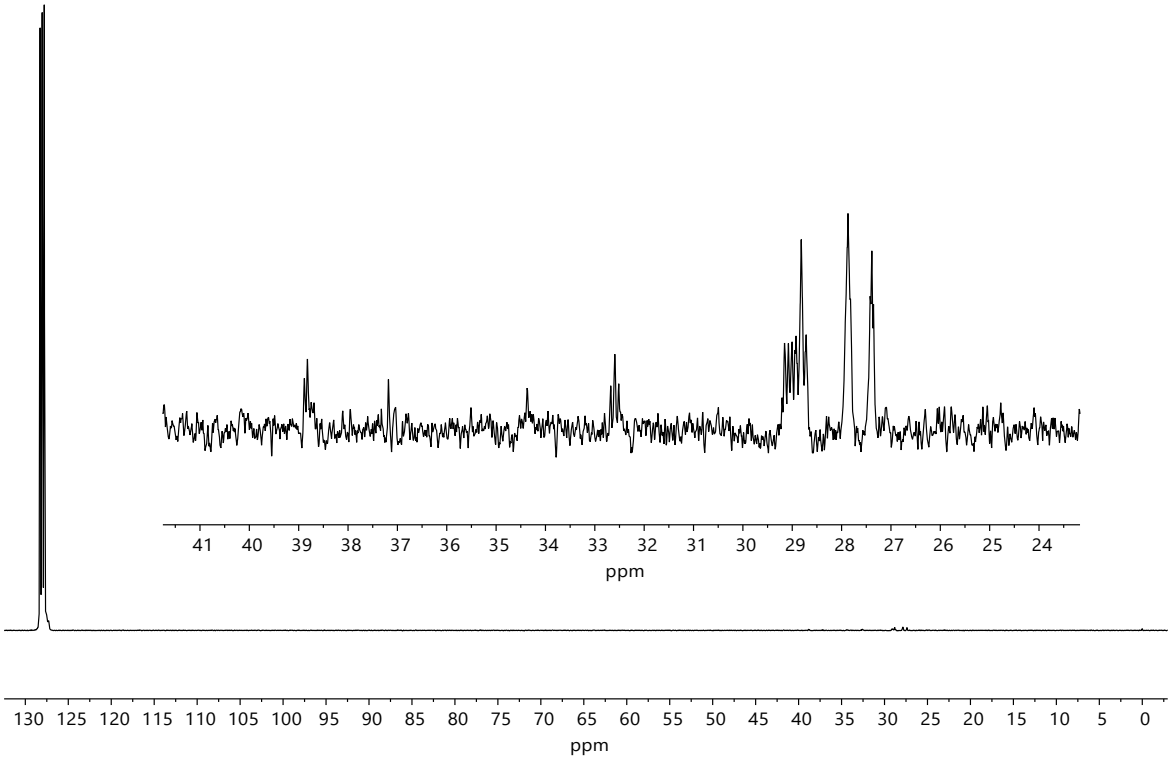

Fig. S19 $^{13}C\{^{1}H\}$ NMR spectrum (101 MHz) of **2**.

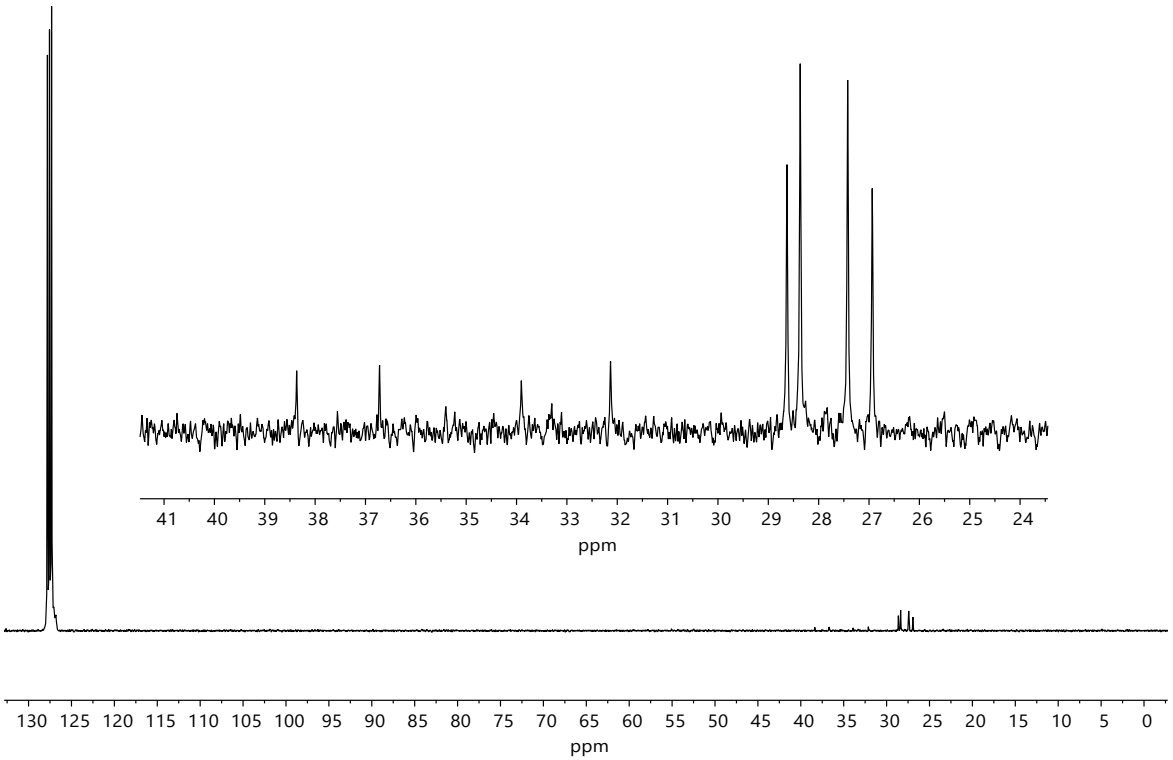

Fig. S20 $^{13}C\{^{1}H,^{31}P\}$ NMR spectrum (101 MHz) of **2** at 28 °C.

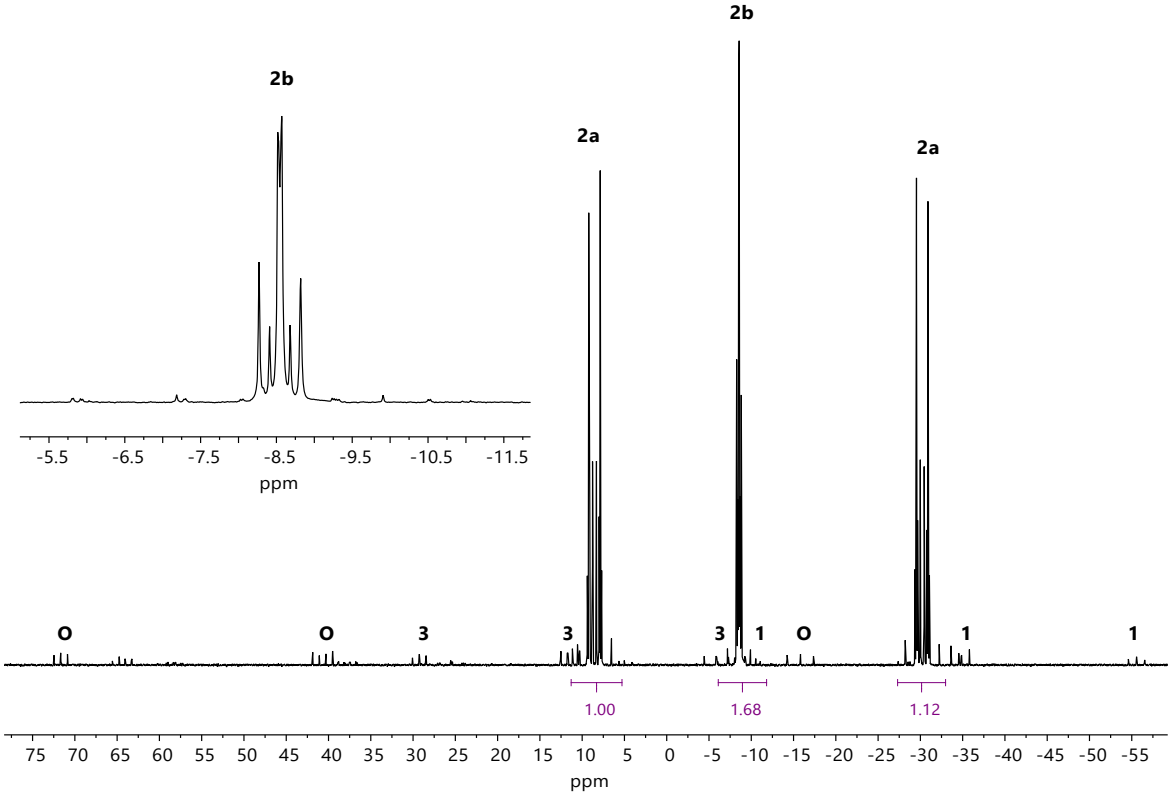

Fig. S21 $^{31}P\{^{1}H\}$ NMR spectrum (162 MHz) of **2** with small amounts of **1** and **3** (equilibrium). The trace impurity **O** is the oxide [1,3-$(AuCl)_2$\{*cyclo*-$(P^tBu)_4$\}O] (**24**).

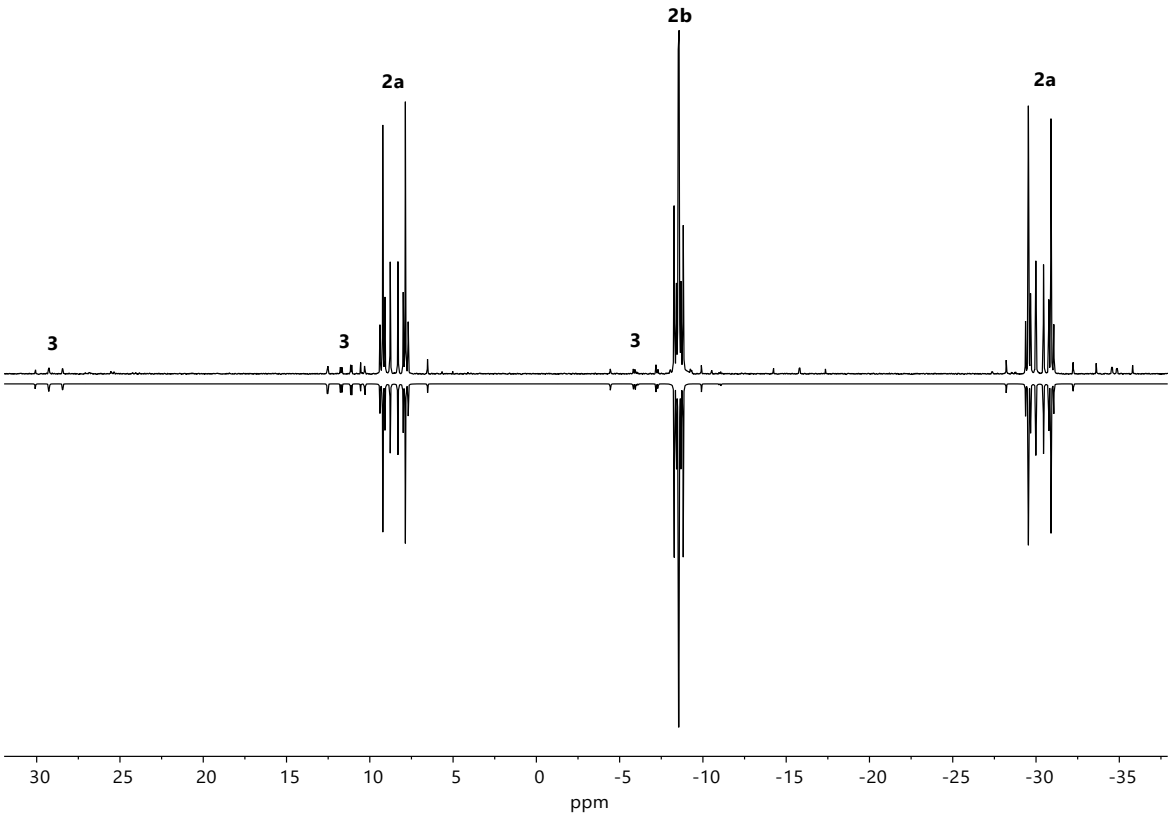

Fig. S22 Experimental (top) and simulated (bottom) $^{31}P\{^{1}H\}$ NMR spectra (162 MHz) of **2a**, **2b** and **3** in benzene-d^6.

$^{31}P\{^{1}H\}$ NMR (162 MHz, benzene-d^6): **2a**: AA'XX' spin system (C_2): $\delta_A = \delta_{A'} = 8.53$, $\delta_X = \delta_{X'} = -30.20$ ppm; $J_{AA'} = -168.59$ Hz, $J_{AX} = -220.31$ Hz, $J_{XX'} = -119.95$ Hz, $J_{AX'} = 0.48$ Hz, $H = 3.34$ Hz; **2b**: A_2B_2 spin system (C_{2v}): $\delta_A = -8.28$, $\delta_B = -8.82$ ppm; $J_{AB} = -206.30$ Hz, $H = 3.0$ Hz; **3**: AM_2X spin system (C_s): $\delta_A = 29.24$, $\delta_M = 11.40$, $\delta_X = -5.82$ ppm; $J_{AM} = -132.74$ Hz, $J_{AX} = -4.96$, $J_{MX} = -230.86$ Hz, $H = 2.85$ Hz. ($R = 0.68$ %)

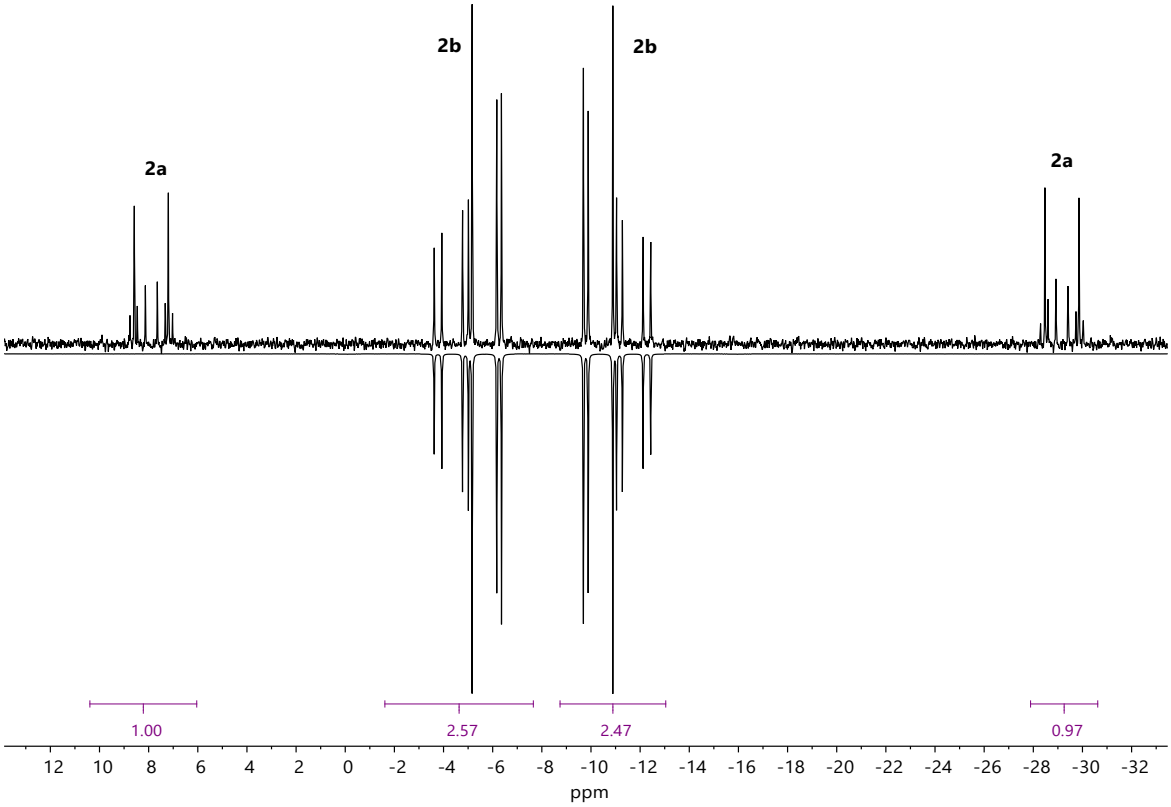

Fig. S23 Experimental $^{31}P\{^{1}H\}$ NMR spectrum (162 MHz) of **2** in acetonitrile-d^3 (top) and simulated (bottom) of **2b**.

$^{31}P\{^{1}H\}$ NMR (162 MHz, acetonitrile-d^3): **2b**: A_2B_2 spin system (C_{2v}, R = 1.03 %): δ_A = –5.16, δ_B = –10.89 ppm; J_{AB} = –206.30 Hz, H = 2.90 Hz.

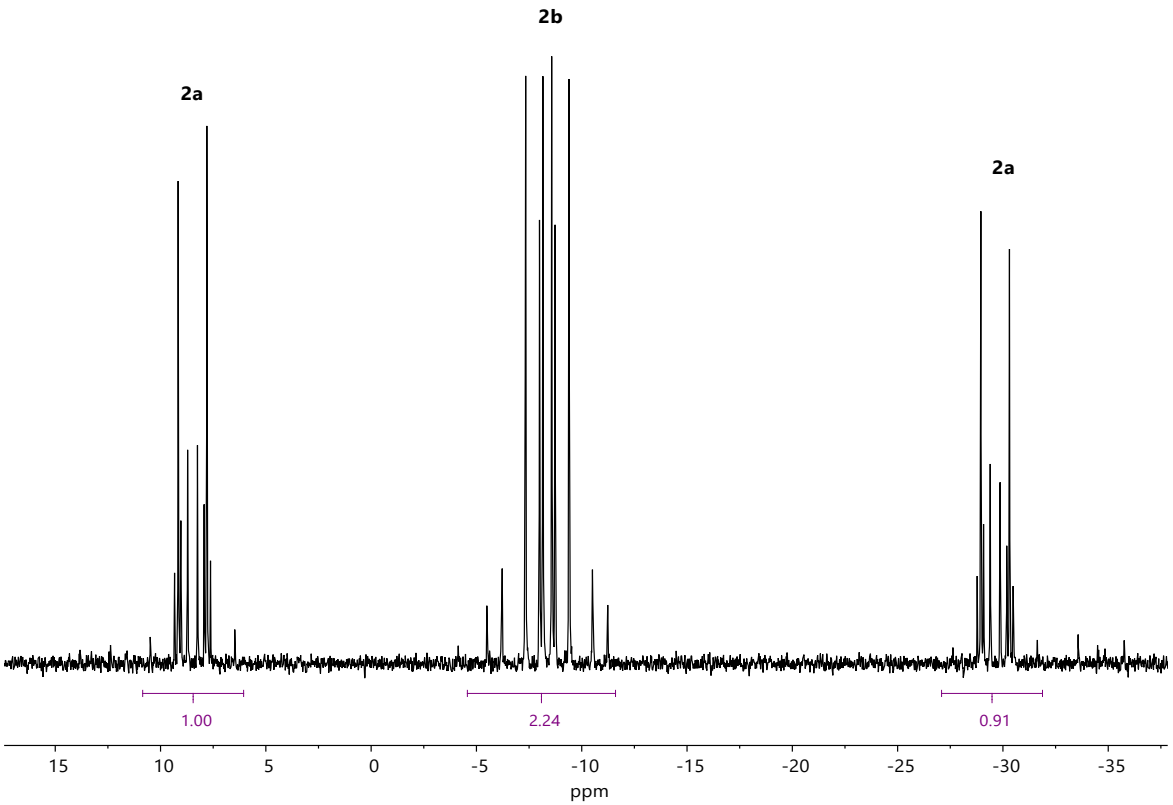

Fig. S24 $^{31}P\{^{1}H\}$ NMR spectrum (162 MHz) of **2** in THF-d^8.

$^{31}P\{^{1}H\}$ NMR (162 MHz, THF-d^8): **2b**: A_2B_2 spin system (C_{2v}, R = 0.52 %): δ_A = –7.34, δ_B = –9.39 ppm; J_{AB} = –202.84 Hz, H = 5.86 Hz.

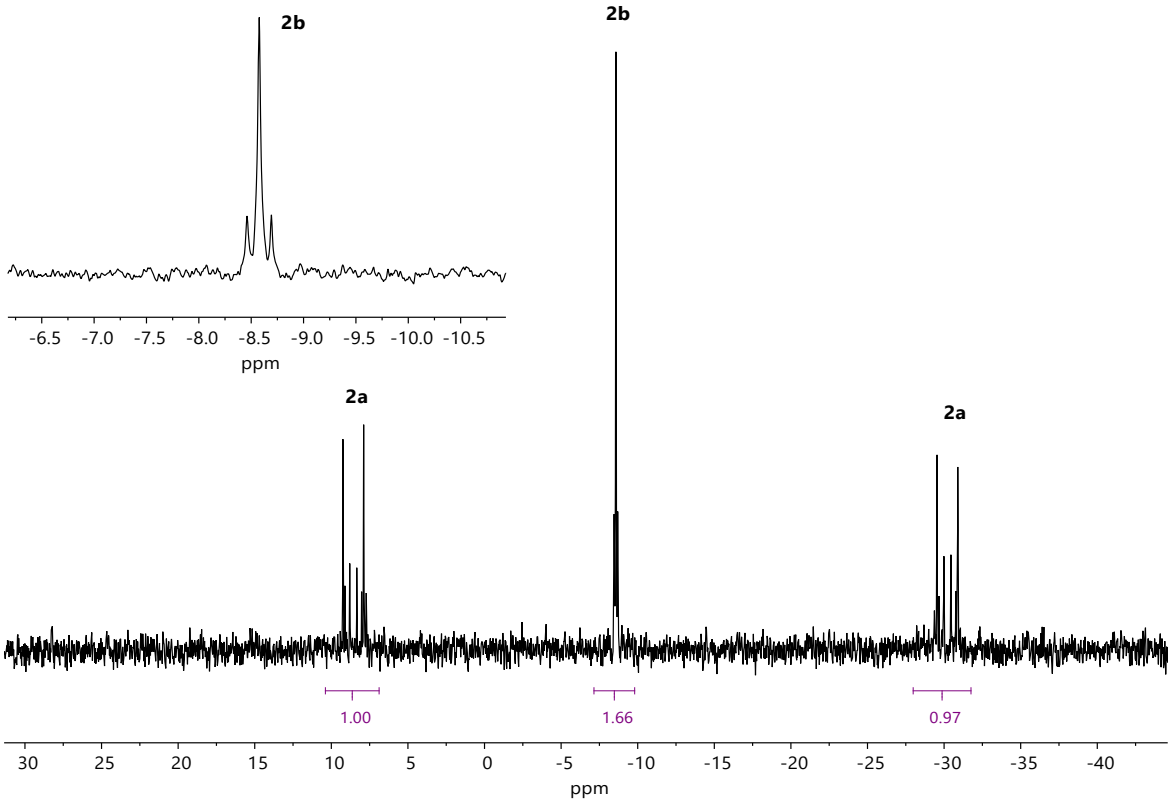

Fig. S25 $^{31}P\{^{1}H\}$ NMR spectrum (162 MHz) of **2** in toluene-d^8.

$^{31}P\{^{1}H\}$ NMR (162 MHz, toluene-d^8): **2b**: A_2B_2 spin system (C_{2v}, R = 0.43 %): δ_A = –8.46, δ_B = –8.69 ppm; J_{AB} = –206.30 Hz, H = 3.79 Hz.

7.3. [(AuCl)$_4${*cyclo*-(P^{t}Bu)$_4$}] (4)

The solid-state $^{31}P\{^{1}H\}$ NMR experiment was performed with an applied MAS rate of 12,500 ± 2 Hz which was controlled by a pneumatic control unit. The temperature of 295.0 K was maintained with a deviation of ±0.2 K by a temperature control unit. Optimised ^{1}H and ^{31}P $\pi/2$ pulse lengths were 2.5 µs and 2.6 µs, respectively. ^{31}P transverse magnetisation created by ramped CP (70–100 %) was transferred from ^{1}H with an optimised contact time of 1 ms and a ^{31}P RF lock field of 38.9 kHz, fulfilling the Hartmann–Hahn condition. The spectrum was recorded with 25,600 scans with a recycle delay of 3.0 s. A Lorentzian apodization function with a line broadening factor of 100 Hz was applied prior to Fourier transformation.

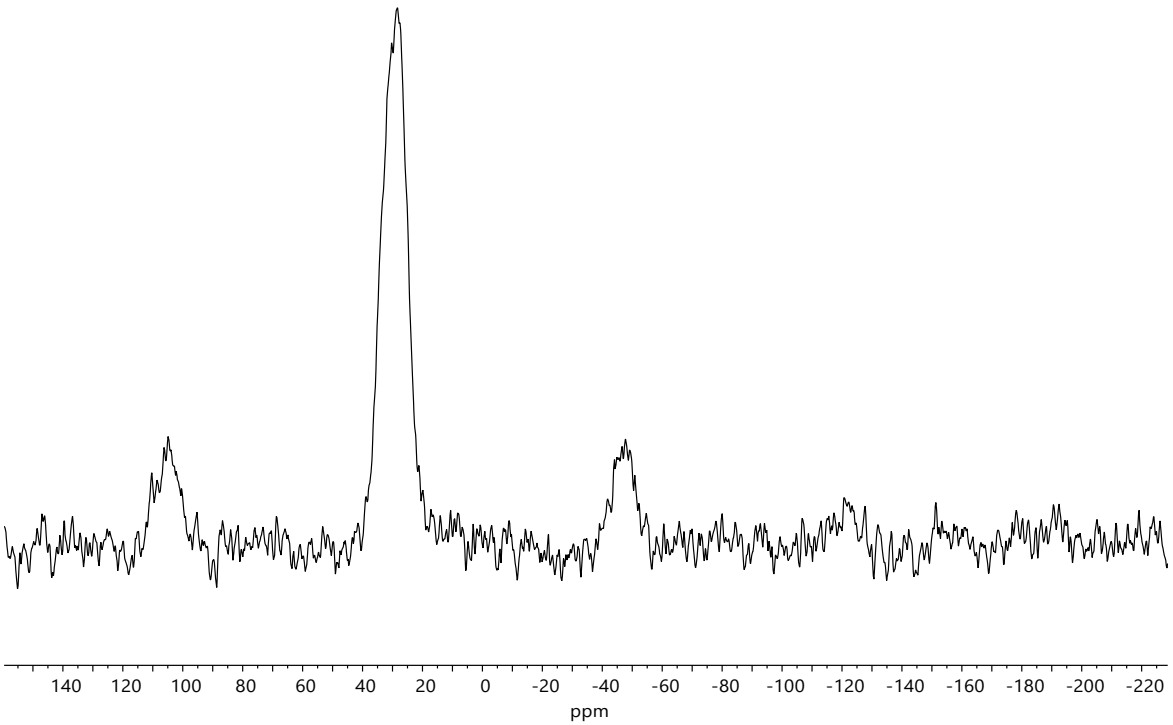

Fig. S26 $^{31}P\{^{1}H\}$ (CP-MAS) spectrum of **4**.

8. References

1 M. Baudler, A. Michels and M. Michels, *Z. Anorg. Allg. Chem.*, 2001, **627**, 31.
2 C. F. Macrae, I. J. Bruno, J. A. Chisholm, P. R. Edgington, P. McCabe, E. Pidcock, L. Rodriguez-Monge, R. Taylor, J. van de Streek and P. A. Wood, *J. Appl. Crystallogr.*, 2008, **41**, 466.
3 *Topas*, Bruker AXS GmbH, Karlsruhe, 2014.
4 F. Neese, *Wiley Interdiscip. Rev.: Comput. Mol. Sci.*, 2018, **8**.
5 E. Caldeweyher, C. Bannwarth and S. Grimme, *J. Chem. Phys.*, 2017, **147**, 34112.
6 E. Caldeweyher, S. Ehlert, A. Hansen, H. Neugebauer, S. Spicher, C. Bannwarth and S. Grimme, *J. Chem. Phys.*, 2019, **150**, 154122.
7 C. van Wüllen, *J. Chem. Phys.*, 1998, **109**, 392.

8 T. Grell and E. Hey-Hawkins, *Eur. J. Inorg. Chem.*, 2020, 720.
9 J. Tao, J. P. Perdew, V. N. Staroverov and G. E. Scuseria, *Phys. Rev. Lett.*, 2003, **91**, 146401.
10 V. N. Staroverov, G. E. Scuseria, J. Tao and J. P. Perdew, *J. Chem. Phys.*, 2003, **119**, 12129.
11 D. A. Pantazis, X.-Y. Chen, C. R. Landis and F. Neese, *J. Chem. Theory Comput.*, 2008, **4**, 908.
12 V. Barone and M. Cossi, *J. Phys. Chem. A*, 1998, **102**, 1995.